Numerical Simulations of Planar Extrusion and Fused Filament Fabrication of Non-Newtonian Fluids

Raphaël Comminal, Jesper H. Hattel, and Jon Spangenberg

Department of Mechanical Engineering, Technical University of Denmark, Kgs. Lyngby, Denmark

ABSTRACT

In this study, the planar extrudate swelling of power-law and Oldroyd-B fluids are investigated. Our numerical predictions are in good agreement with the other results available in the literature. In addition, a simplified two-dimensional model of fused filament fabrication that provides details of the flow in the gap between the printing head and the substrate is presented. The numerical simulations use the streamfunction/log-conformation and the volume-of-fluid methods.

INTRODUCTION

The simulation of non-Newtonian free-surface flows is an important topic of computational rheology. The free-surface flow simulations of non-Newtonian fluids have several applications in polymer processing. Extrusion and fused filament fabrications are two examples of these applications related to the manufacturing of plastic parts. Fused filament fabrication is a popular 3D-printing technique, based on the extrusion of a molten filament deposited on a moving substrate. In this technology, the size of printed filament is a key fabrication parameter, as it both determines the fabrication time and the precision of the 3D print.

The optimal processing parameter often depends on the rheology of the material. Numerical simulations can help understanding the flow mechanism. Shape optimization algorithms and sensitivity analysis built on numerical simulations have successfully been applied to develop computer-aided design strategies for extrusion dies[1,2,3].

Generally, non-Newtonian fluids are either characterized by a non-constant viscosity that depends on the flow conditions (shear-thinning and pseudo-plastic liquids), or by a time-dependent stress response that includes an elastic stress component representing the recoverable deformations coming from the stretching of polymer chains (viscoelastic liquids). Extrudate swelling is a typical phenomenon influenced by shear-thinning and viscoelasticity.

This conference paper presents numerical results of two-dimensional simulations of the extrudate swelling and the fused filament fabrication of non-Newtonian fluids. The models focus on the flow regions near the die exits. The results are computed with a novel non-Newtonian flow solver, based on the streamfunction/log-conformation method of Comminal et al.[4,5].

GOVERNING EQUATIONS

The isothermal creeping flows of the incompressible non-Newtonian fluids are governed by the conservation of mass and momentum:

$$\nabla \cdot \mathbf{u} = 0 \tag{1}$$

$$\rho \frac{\partial \mathbf{u}}{\partial t} = -\nabla p + \nabla \cdot \boldsymbol{\tau} \tag{2}$$

where $\mathbf{u}$ is the velocity field, $\boldsymbol{\tau}$ is the internal stress, p is the isostatic pressure, ρ is the density, and t is the time variable. The momentum convection terms in Eq. 2 are neglected, because of the assumption of a creeping flow. However, the time derivative $\left(\partial \mathbf{u}/\partial t\right)$ is kept in Eq. 2, because of possible transient stress responses of the non-Newtonian (viscoelastic) fluids. The conservation laws are closed by the constitutive model, which links the internal stress to the strain-rate tensor

$$\mathbf{D} = \frac{1}{2}\left(\nabla \mathbf{u} + \nabla \mathbf{u}^{\mathrm{T}}\right) \tag{3}$$

Several constitutive models are considered. The non-Newtonian materials with instantaneous stress responses are represented with the generalized Newtonian fluid model:

$$\boldsymbol{\tau} = 2\eta\left(I_2^{\mathbf{D}}\right)\mathbf{D} \tag{4}$$

where $\eta\left(I_2^{\mathbf{D}}\right)$ is the apparent viscosity of the material, which may depend on the invariants of the strain-rate tensor. The first invariant $I_1^{\mathbf{D}} = \mathrm{tr}\left(\mathbf{D}\right)$ is zero, because of the incompressibility constraint (Eq. 1). The second invariant is given by:

$$I_2^{\mathbf{D}} = \mathrm{tr}\left(\mathbf{D}^2\right) = \sum_i \sum_j D_{ij} D_{ji} \tag{5}$$

In our study, the apparent viscosity is modelled with the Carreau fluid model:

$$\eta\left(I_2^{\mathbf{D}}\right) = \eta_0 \left(1 + \left(k\dot{\gamma}\right)^2\right)^{\frac{n-1}{2}} \tag{6}$$

where $\dot{\gamma} = \sqrt{I_2^{\mathbf{D}}}$ is the magnitude of the shear-rate tensor in the Frobenius norm, and η_0, k and n are material properties. The Carreau fluid model typically predicts a smooth transition between a plateau viscosity η_0, for $k\dot{\gamma} \ll 1$, and a power-law behaviour with power-index n, for $k\dot{\gamma} \gg 1$. However, we intentionally chose a very low value for k $\left(=10^{-6}\right)$, and a large value for η_0 $\left(=10^{8}\right)$, such that the Carreau model essentially behaves as a power-law fluid with a consistency $K = \eta_0 k^{n-1}$, and a maximum cut-off value of the apparent viscosity $\eta_{\max} = \eta_0$, when the flow is close to the quiescent state. The Newtonian fluid model recovered for $n = 1$.

Materials with time-dependent stress responses are modeled with viscoelastic constitutive models. We consider the case of a linear viscoelastic material described by Oldroyd-B model:

$$\boldsymbol{\tau} = \boldsymbol{\tau}_{\mathrm{N}} + \boldsymbol{\tau}_{\mathrm{E}} \tag{7}$$

where

$$\boldsymbol{\tau}_{\mathrm{N}} = 2\beta\eta\mathbf{D} \tag{8}$$

is the instantaneous (purely viscous) stress response of the material, and

$$\boldsymbol{\tau}_{\mathrm{E}} = \frac{\left(1-\beta\right)\eta}{\lambda}\left(\mathbf{c} - \mathbf{I}\right) \tag{9}$$

and $\boldsymbol{\tau}_{\mathrm{E}}$ is the time-dependent extra-stress contribution. The extra-stress tensor is related to the conformation tensor $\mathbf{c}$, representing the internal elastic strain of the liquid. The constant viscosity η, the retardation ratio β, and the relaxation time λ are material parameters, while $\mathbf{I}$ is the identity matrix.

The conformation tensor is governed by the following partial differential equation:

$$\overset{\nabla}{\mathbf{c}} = -\frac{1}{\lambda}\left(\mathbf{c}-\mathbf{I}\right) \tag{10}$$

where

$$\overset{\nabla}{\mathbf{c}} \equiv \frac{\partial \mathbf{c}}{\partial t} + \mathbf{u}\cdot\nabla\mathbf{c} - \left(\mathbf{c}\cdot\nabla\mathbf{u}^{\mathrm{T}} + \nabla\mathbf{u}\cdot\mathbf{c}\right) \tag{11}$$

is the upper-convective time-derivative, which accounts for the material transport and the frame-invariance of the conformation tensor.

The relative effect of the elastic stresses, as compared to the viscous stresses, is quantified by the dimensionless Weissenberg number Wi, defined as:

$$Wi = \lambda\dot{\gamma}_c \tag{12}$$

where $\dot{\gamma}_c$ is the characteristic shear-rate of the flow. The retardation ratio β is also a dimensionless parameter controling the fractions of the viscosity that contribute to the instantaneous and the time-dependent stress responses.

NUMERICAL METHOD

The non-Newtonian free-surface flow is simulated as a two-phase flow, where the second phase corresponds to the air surrounding the liquid. The volume-averaged governing equations of the two-phase flow are solved with the numerical scheme proposed by Comminal et al.[4,5]. The partial differential equations are discretized with the finite-volume method, on staggered Cartesian grids. An implicit second-order accurate scheme is obtained by using the two-level backward differentiation formula for the temporal differentiations, centred finite-differences for the diffusion fluxes, and the CUBISTA interpolation scheme[6] for the advection fluxes.

The linear system of the discretized conservation equations is solved with the exact fractional step method of Chang et al.[7]. On the discrete level, this exact fractional step method is equivalent to the pure streamfunction formulation[8], where the conservation laws are solved in the curl form. This exact projection method enforces by construction the mass conservation. Moreover, the streamfunction formulation is particularly advantageous in the 2D case, as it reduces the number of unknowns.

The components of the extra-stress tensor of the viscoelastic fluids are solved with the log-conformation representation method of Fattal and Kupferman[9,10]. The non-linearity between the velocities and the extra-stresses are solved with successive substitution iterations.

The position of the free-surface is captured with the volume-of-fluid method and a piecewise linear interface reconstruction[11]. The liquid volume fraction of the non-Newtonian phase is advected with the cellwise conservative unsplit geometrical advection scheme proposed by Comminal et al.[12].

SIMULATION RESULTS

This section presents numerical results of the planar extrusion and a simplified model of fused filament fabrication.

Planar extrusion

The planar extrudate swelling of power-law and Oldroyd-B fluids exiting a slit die were simulated for various power-indices and Weissenberg numbers, respectively. The retardation ratio of the Oldroyd-B fluid was set constant to the value $\beta = 1/9$, in all the simulations.

The geometry of the simulations consisted in the union of two rectangular domains representing the slit extrusion die and the planar expansion at the die exit. By virtue of symmetry, we only simulate half of

the geometry. A fully-developed flow is imposed at the inlet boundary of the die, while the outlet boundary far away from the die exit is constrained by the Neumann boundary condition. The no-slip boundary condition is applied at the wall of the die and the expansion plane. At the exit of the die, the parabolic fully-developed flow profile gets rearranged into a plug flow profile with a uniform velocity. The extrudate swelling Sr is defined as the ratio of the extrudate thickness D_{extr} by the die's width D_{die}:

$$Sr = \frac{D_{\text{extr}}}{D_{\text{die}}} \tag{13}$$

The planar extrusion was simulated on two different grids: a coarse mesh and a fine mesh. The grid spacing of the fine mesh is half of the grid spacing of the coarse one. Both grids present a contraction of their grid spacing near the die exit (where large strain-rate are expected) in both directions.

The numerical results of the extrudate swelling of the power-law fluids with various power-indices are reported in Fig. 1. As expected, the shear-thinning reduces the extrudate swelling. The fully-developed flow profile of the power-law fluid is:

$$U(y) = \frac{2n+1}{n+1}\left[1-\left(y/h\right)^{\frac{n+1}{n}}\right]U_0 \tag{14}$$

where y is the distance to the midline, $h = D_{\text{die}}/2$ is the half width of the die, and U_0 is the average velocity of the fully-developed flow, see Fig. 2. The flow profile becomes closer to a plug flow profile, when the power-index is reduced (enhancing shear-thinning). Thus, the flow profile requires less rearrangement at the die exit, which ultimately reduces extrudate swelling.

For the Oldroyd-B liquid, the fully-developed creeping flow profile is identical to the Newtonian fluid. However, the Oldroyd-B liquid also develops a normal stress difference N_1 inside the die, in addition to the shear stress τ. The normal stress difference come from the elastic effects in the viscoelastic liquid. At the die exit, the relaxation of the elastic stresses, contributes to the extrudate swelling. Hence, the swelling ratio increases with the Weissenberg number $Wi = 3\lambda U_0/h$ (here the relaxation time is normalized by the shear-rate at the wall $\dot{\gamma}_w = 3U_0/h$).

The different fields of the conformation tensor components are plotted in Fig. 3, for $Wi = 2$. The data shows a stress singularity

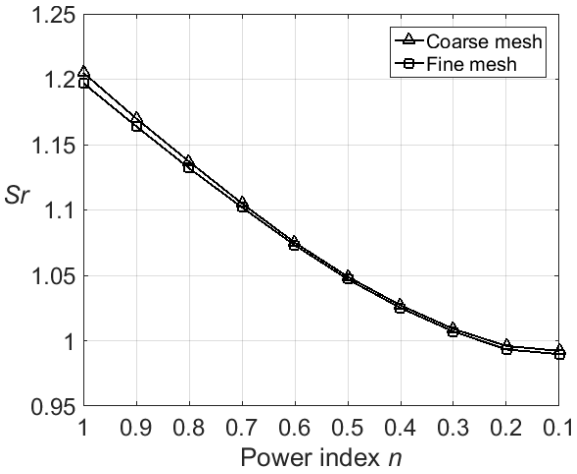

Figure 1. Extrudate swell of the power-law fluid as a function of the power-index n.

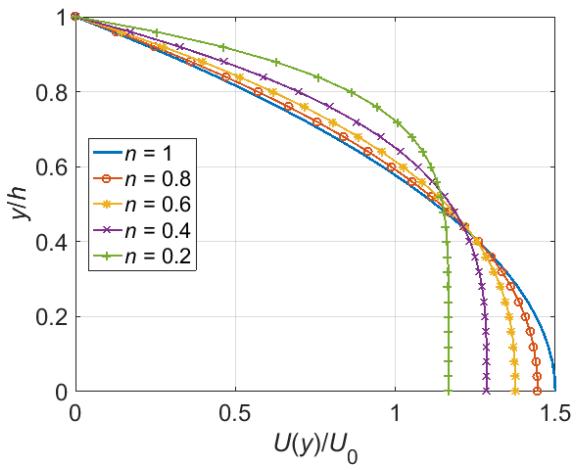

Figure 2. Fully-developed creeping flows profile of the power-law fluids.

at the corner of the die. (For more clearness, the maximal values of the colorbars have been cut-off below the maximum values of the conformation tensor.) We can also see large tensile stresses in the skin layer of the extrudate, just after the die exit.

The extrudate swelling of the Oldroyd-B liquid are represented in Fig. 4, together with other numerical solutions available in the literature. We must notify that our numerical solutions contain some small oscillations of the free-surface, at $Wi = 2.5$ and $Wi = 3$, for the fine mesh only. These surface oscillations are numerical artefacts coming from the under-resolution of the flow at the tip of the free-surface on the expansion plane, when the tangent of the contact angle is larger than the aspect ratio of the grid cells. The results presented in Fig. 4 corresponds to the averaged swelling ratio, far away from the die exit.

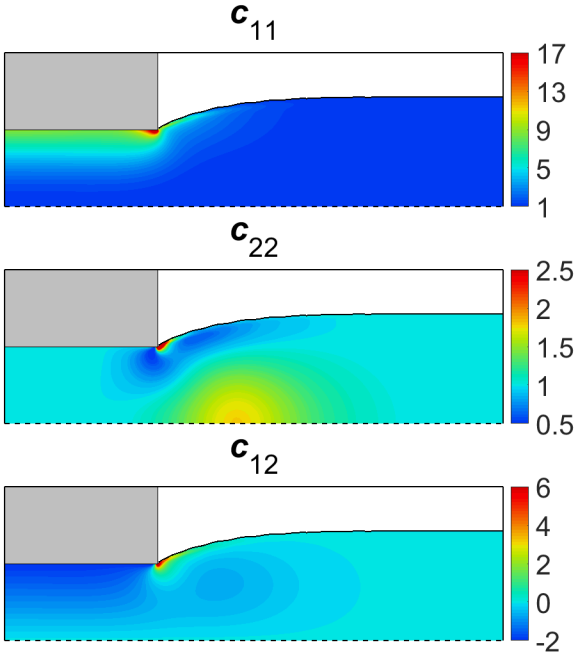

Figure 3. Fields of the conformation tensor components at the die exit, for $Wi = 2$ and $\beta = 1/9$ (calculated on the fine mesh).

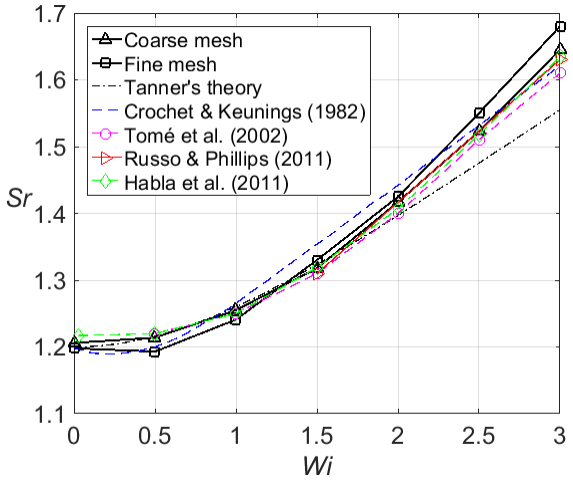

Figure 4. Extrudate swell of the Oldroyd-B liquid as a function of Wi (with $\beta = 1/9$).

Deviations between the different numerical results plotted in Fig. 4 are noticeable, for $Wi \geq 2.5$; however, for the low Wi numbers, the numerical solutions are in good agreements. Crochet and Keunings[13] implemented a Lagrangian finite-element scheme with a deforming mesh to calculate the steady-state solution of the extrudate swelling problem. Russo and Phillips[14] used the spectral element method and the arbitrary Lagrangian Eulerian technique. Tomé et al.[15] solved the extrudate swelling with a Eulerian transient free-surface flow solver based on the marker-and-cell method, which was specially developed for non-Newtonian fluids. The results of Habla et al.[16] were obtained with an extension of the open-source software OpenFOAM®, where the volume-of-fluid method is used to model the free-surface flows as two-phase flows. The numerical results are also compared with the approximated analytical solution of Tanner[17]:

$$Sr = 0.12 + \left(1 + \frac{S_w^{\,2}}{3}\right)^{1/4} \qquad (15)$$

where $S_w = N_1/2\tau = \beta Wi$ is the recoverable shear at the walls of die, and the term 0.12 correspond to the swelling of a Newtonian fluid in a creeping flow. At low Wi, the analytical and numerical solutions are in good agreement. However, the assumptions in Tanner's theory are only valid for low values of Wi. This explains the divergence between Tanner's analytical solution and the numerical results, when $Wi \geq 2$.

Fused filament fabrication

We present a simplified model of extrusion-based 3D-printing that focuses on the flow at the exit of the printing nozzle. The numerical model consists in a two-dimensional channel (representing the nozzle) that faces a moving surface (representing the substrate). The geometry is characterized by the diameter d of the nozzle and the gap g between the printing head and the moving surface. An inlet boundary condition with a fully-developed creeping flow profile is applied within the channel. The moving surface is assigned a tangential velocity V. The velocity of the moving surface is normalized by the average velocity U_0 of the fluid inside the nozzle. The shape of the two-dimensional printed filament exiting the nozzle has been simulated, for different values of the gap and the velocities of the moving table; see the snapshots of the results in Fig. 5. In these numerical simulations, the printed material was modelled as a Newtonian fluid. Within this simplified two-dimensional model, the thickness δ of the printed filament is simply determined by the mass conservation, independently of the rheology of the fluid. The throughput $\delta \times V$ of the printed filament must equal the influx $d \times U_0$ of the inlet boundary of the nozzle. Therefore, we have the following relation:

$$\delta = \frac{dU_0}{V} \qquad (16)$$

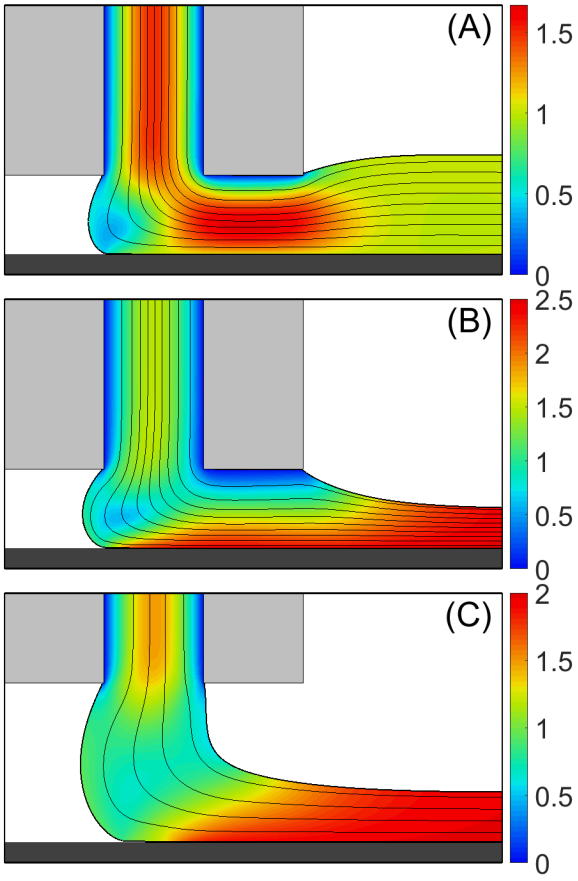

Figure 5. Streamlines and normalized velocity fields at the exit of the printing nozzle, for various processing parameters: (A) $g/d = 0.8$, $V/U_0 = 1.0$; (B) $g/d = 0.8$, $V/U_0 = 2.5$; (C) $g/d = 1.6$, $V/U_0 = 2.0$.

As expected, the numerical simulations of the Newtonian fluid predict the correct filament's thickness; see the results plotted in Fig. 6. Nevertheless, if a prescribed force was applied at the inlet boundary, instead of the prescribed velocity, then the average velocity U_0 would be an unknown of the model that depends on the rheology of the fluid. In that case, an analytical solution of the filament's thickness could be derived on the same line as Jabbari et al.[18], who predicted the thickness of a shear-thinning slurry in tape casting. The analytical solutions of Cruz et al.[19] may also be useful, in case of a viscoelastic liquid.

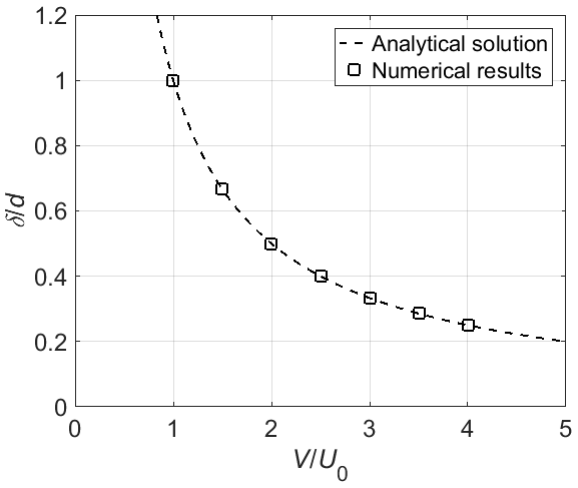

Figure 6. Analytical and numerical predictions of the filament's thickness as a function of the velocity of the moving table, within the simplified two-dimensional model.

CONCLUSION

An in-house non-Newtonian free-surface flow solver, based on the volume-of-fluid method and the streamfunction/log-conformation formulation, has been developed for this study. The planar extrudate swelling of the power-law and the Oldroyd-B fluids have been calculated for different values of the power-index and the Weissenberg number, respectively. Our predictions are in relatively good agreement with other results available in the literature.

A simplified two-dimensional model of the fused filament fabrication was also presented. This model provides details of the flow in the gap between the printing head and the substrate. However, due to the prescribed influx boundary condition, the thickness of the printed filament solely depends on the velocity of the moving table, by virtue of mass conservation. Hence, a different boundary condition (for instance a prescribed pressure) must be applied at the inlet boundary, in order to investigate the effect of the rheology on the filament's thickness. Finally, further studies should also consider the non-isothermal effects of the molten material.

ACKNOWLEDGMENTS

The authors acknowledge fruitful discussions with Prof. M.A. Alves from U. Porto, regarding the simulations of the extrudate swelling.

REFERENCES

1. Lebaal, N., Schmidt, F., and Puissant, S. (2009), "Design and optimization of three-dimensional extrusion dies, using constraint optimization algorithm", *Finite Elem. Anal. Des.*, **45**, 333-340.

2. Elgeti, S., Probst, M., Windeck, C., Behr, M., Michaeli, W., and Hopmann, C. (2012), "Numerical shape optimization as an approach to extrusion die design", *Finite Elem. Anal. Des.*, **61**, 35-43.

3. Pauli, L., Behr, M., and Elgeti, S. (2013), "Towards shape optimization of profile extrusion dies with respect to homogeneous die swell", *J. Non-Newtonian Fluid Mech.*, **200**, 79-87.

4. Comminal, R., Spangenberg, J., and Hattel, J.H. (2015), "Robust simulations of viscoelastic flows at high Weissenberg numbers with the streamfunction/log-conformation formulation", *J. Non-Newtonian Fluid Mech.*, **223**, 37-61.

5. Comminal, R., Hattel, J.H., Alves, M.A., and Spangenberg, J. (2016), "Vortex behavior of the Oldroyd-B fluid in the 4-1 planar contraction simulated with the streamfunction–log-conformation formulation", *J. Non-Newtonian Fluid Mech.*, **237**, 1-15.

6. Alves, M.A., Oliveira, P.J., and Pinho, F.T. (2003), "A convergent and universally bounded interpolation scheme for the treatment of advection", *Int. J. Numer. Meth. Fluids*, **41**, 47-75.

7. Chang, W., Giraldo, F., and Perot, B. (2002), "Analysis of an exact fractional step method", *J. Comput. Phys.*, **180**, 183-199.

8. Kupferman, R. (2001), "A central-difference scheme for a pure stream function formulation of incompressible viscous flow", *SIAM J. Sci. Comput.*, **23**, 1-18.

9. Fattal, R., and Kupferman, R. (2004), "Constitutive laws for the matrix-logarithm of the conformation tensor", *J. Non-Newtonian Fluid Mech.*, **123**, 281-285.

10. Fattal, R., and Kupferman, R. (2005), "Time-dependent simulation of viscoelastic flows at high Weissenberg number using the log-conformation representation", *J. Non-Newtonian Fluid Mech.*, **126**, 23-37.

11. Rider, W.J., and Kothe, D.B. (1998), "Reconstructing volume tracking", *J. Comput. Phys.*, **141**, 112-152.

12. Comminal, R., Spangenberg, J., and Hattel, J.H. (2015), "Cellwise conservative unsplit advection for the volume of fluid method", *J. Comput. Phys.*, **283**, 582-608.

13. Crochet, M.J., and Keunings, R. (1982), "Finite element analysis of die swell of a highly elastic fluid", *J. Non-Newtonian Fluid Mech.*, **10**, 339-356.

14. Russo, G., and Phillips, T.N. (2011), "Spectral element predictions of die-swell for Oldroyd-B fluids", *Comput. Fluids*, **43**, 107-118.

15. Tomé, M.F., Mangiavacchi, N., Cuminato, J.A., Castelo, A., and McKee, S. (2002), "A finite difference technique for simulating unsteady viscoelastic free surface flows", *J. Non-Newtonian Fluid Mech.*, **106**, 61-106.

16. Habla, F., Marschall, H., Hinrichsen, O., Dietsche, L., Jasak, H., and Favero, J.L. (2011), "Numerical simulation of viscoelastic two-phase flows using openFOAM®", *Chem. Eng. Sci.*, **66**, 5487-5496.

17. Tanner, R.I. (2005), "A theory of die-swell revisited", *J. Non-Newtonian Fluid Mech.*, **129**, 85-87.

18. Jabbari, M., Bulatova, R., Hattel, J.H., and Bahl, C.R. (2013), "Quasi-steady state power law model for flow of $(La_{0\cdot85}Sr_{0\cdot15})_{0\cdot9}MnO_3$ ceramic slurry in tape casting", *Mater. Sci. Technol.*, **29**, 1080-1087.

19. Cruz, D.O., Pinho, F.T., and Oliveira, P.J. (2005), "Analytical solutions for fully developed laminar flow of some viscoelastic liquids with a Newtonian solvent contribution", *J. Non-Newtonian Fluid Mech.*, **132**, 28-35.